

行政院原子能委員會
委託研究計畫研究報告

利用影像回授技術進行輔助控制之研究
Study on Using Visual Feedback Technique to Assist Control

計畫編號：1012001INNER003
受委託機關（構）：中原大學
計畫主持人：張政元
聯絡電話：03-2654838
E-mail address：ccy@cycu.edu.tw
核研所聯絡人員：黃崇豪
報告日期：101年11月12日

目 錄

目 錄.....	ii
中文摘要.....	1
Abstract.....	2
計畫參與人員及所屬單位.....	3
壹、計畫緣起與目的.....	4
貳、研究方法與過程.....	6
參、實驗結果.....	14
肆、結論.....	18
參考文獻.....	19
附錄、機械手臂之控制設計與模擬分析.....	21

中文摘要

高活度大型核能組件的切割需要利用遙控技術來操作吊車或機械手臂等器械，並在這些器械上固定切割工具以進行施工，然而，實施這些技術時，器械本身所使用的感測器(如編碼器)或機件結構的影響會有量測誤差的問題，因此，會對系統的定位控制產生不利的影響；故對於感測器量測的準確性來說亟需詳加探討。本計畫主要希望裝置一個影像輔助裝置來進行回授控制，利用操控技術將吊車或機械手臂移至目標點附近時，能切換至影像回授控制，來改善原本的失真誤差問題，以建立更精確的控制技術。這個技術主要是將所擷取的影像自動進行辨識，以瞭解目前切割工具的所在位置與目標位置的距離與方位，進而依此數據計算操控量以操作吊車或機械手臂等器械。此外，有關影像裝置的各類失真補償研究也會在計畫中規劃與討論，俾利於進行本所及國內大型核能組件拆除。

關鍵字: 吊車、量測誤差、影像回授、失真誤差

Abstract

In general, removing the core components of nuclear power mechanism needs to remote control the crane or robot arm. However, the encoders, sensors to measure the crane position and load sway, could be not precise due to the vibration of motion or other factors. Therefore, it is not easy to control the crane well with the measurement error. This project tries to develop a switching method to control the crane. And utilize error-free image sensor when the crane motion is close to the destination to derive the precise control signal. So, the control signal can provide correct information to stop the crane at destination. The proposed technique not only can identify necessary information from the image automatically to realize the position and swing angle of the crane. In addition, the problem of nonlinear distortion of image processing will also be studied in this project for removing the core components of nuclear power mechanism safely and smoothly.

Keywords: crane, measurement error, image sensor, error and distortion.

計畫參與人員及所屬單位

計畫編號：1012001INER003

計畫參與人員：張政元¹、蔣東建²、古松志¹、楊志恆¹

所屬單位：中原大學電機系¹、健行科大電子系²

壹、計畫緣起與目的

Conventional control applications often utilized encoders to track the mechanical motion. However, using encoders may lead to inaccuracy. Main measurement errors aroused from encoder aging or designing problems of mechanism such as vibration. These problems deteriorate the performance of control system. Therefore, using digital image sensor to visual feedback control is a potential solution for industrial applications. Some papers have been published on visual tracking and implemented on some applications. However, many visual tracking only used to recognize an object, like ball, human and face etc [1]-[4], but not in visual feedback for control problems. Besides, many researcheres focused in simple mechanical systems like inverted pendulum with visual feedback control [5]-[8], but it lacked to prove their performance for complex system.

Few researches attracted to implement image sensing to measure the swing angle of the overhead crane. Kawai et al. [9] installed a camera at the cart of the crane to measure the swing angle. This kind of installation does not free the camera from displacement caused by the vibration of the cart. Osumi et al. [10] used two CCD to calculate the angle of the swing, but it took 31ms to calculate it. Miyamoto et al. [11] used laser to detect a cross mark at the crane hook. These researches also did not test their performance in real-time. Moreover, Matsuo et al. [12] implemented visual feedback on PID+Q controller for the crane controller using a built-in video tracker. Yoshida and Tsuzuki [13] made an anti-swing of the overhead crane with visual feedback using stereovision camera that mounted on the robot, which costs a lot.

In general, the main constraint of a visual feedback control system is the computation time [3]. Besides, a fast algorithm is highly required to deal with real-time data for the feedback control algorithm. Therefore, some industrial applicators used an expensive high-end computational technology to improve the

processing time. A high-speed camera also used by many applicators to handle the real time tracking task. Thus the cost of overall control system is very high. In contrary, this manuscript builds a visual feedback control system with a 30 frame per second (fps) handy camcorder and basic personal computer without any increased hardware. A visual tracking based on color histogram has been implemented on this system. Fast recognition and multiple localization of the object are the advantages of this algorithm, which are also needed in this system. It matches the color histogram of the model with the color histograms in the image sequences. To achieve the maximum performance of camcorder, we propose an algorithm which does not process a whole image. It is limited only within the size of the tracking blocks. A block will move and follows the object that we tracked. Therefore, the proposed visual tracking method can be used to replace physical sensor like encoder. It tracks down the rope and the load to give the precise angle and position of the load data. The comparisons with the existing method with physical sensor verify the effectiveness of the proposed visual tracking technique.

貳、研究方法與過程

2.1.1. Color histograms tracking

A color histogram is a representation of the distribution of colors for a digital image. It is basically the number of pixels that has colors in each of a fixed list of color ranges spanning the color space of image. The color histogram can be built for any kind of color space, although the term is often used for three-dimensional spaces like RGB or HSV. By the way, RGB color spaces were employed in this manuscript that directly captured by the camera. Like other kinds of histograms, the color histogram is a statistic that can be viewed as an approximation of an underlying continuous distribution of colors values. By mapping the colors in an image into a discrete color space containing n colors, a color histogram $H(M)$ is a vector (h_1, h_2, \dots, h_n) in a n -dimensional vector space, where each element h_i represents the number of pixels of color i in the image M . Equation (1) represents a one-dimensional color histogram that is R, G and B of the image in every pixel in the image [1]

$$q^R = \{q_r^R\}, q^G = \{q_g^G\}, q^B = \{q_b^B\} \quad (1)$$

where $r = 1, 2, \dots, R$; $g = 1, 2, \dots, G$; $b = 1, 2, \dots, B$, with q_r^R, q_g^G, q_b^B represent the number of pixels (x, y) in the image. The values of red in the bin of r , the values of green in the bin of g , and the values of blue in the bin b . The notation R , G , and B are the number of bins of red, green, and blue, respectively.

A color contains data that can be very useful to be used on object tracking. A histogram of the color is independent from the scaling and rotation of the object. In this experiment, a visual tracking based on color histograms used to track the target. The color histogram tracker works by first creating a color histogram of a fixed sub-region of the image; presumably in the immediate neighborhood of the target to be tracked, which we refer as the model histogram patch, like illustrated in Fig. 1, a model color histogram of a table tennis ball. During the tracking stage, every incoming frame from the camera is divided into rectangular regions and their

histograms are calculated.

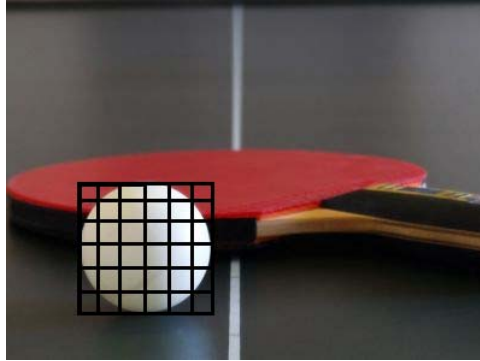


Fig. 1: A model color histogram

The similarities between the new candidate histogram in image sequences and the model histogram are calculated by Bhattacharyya similarity as explained in the next sub section. The sub-window with the highest match is chosen as the probable target. The pattern of scanning the image for the target can be done sequentially, and the size and shape of the sub-window can also be made to change dynamically.

2.1.2. Bhattacharyya similarity on color histograms

Bhattacharyya's original interpretation of the measure was geometric. We considered two multinomial populations each consisting of k categories classes with associated probabilities (p_1, p_2, \dots, p_k) and (q_1, q_2, \dots, q_k) , respectively. Then, normalized as $\sum_{i=1}^k p_i = 1$ and $\sum_{i=1}^k q_i = 1$, we noted that $(\sqrt{p_1}, \sqrt{p_2}, \dots, \sqrt{p_k})$ and $(\sqrt{q_1}, \sqrt{q_2}, \dots, \sqrt{q_k})$ could be considered as the direction cosines of two vectors in k -dimensional space referred to a system of orthogonal co-ordinate axes. As a measure of divergence between the two populations Bhattacharyya used the square of the angle between the two position vectors. If θ is the angle between the vectors then:

$$\cos \theta = \sum_{i=1}^k \sqrt{p_i q_i} = \rho \quad (2)$$

Thus if the two populations are identical, then $\rho = \cos \theta = 1$, corresponding to $\theta = 0$, where ρ is known as Bhattacharyya coefficient for the similarity. Therefore, it will be used to measure the similarity of the color distribution in RGB color space between the model image and image sequences

$$\rho^R = \sqrt{p^R(x, y)q^R}, \quad \rho^G = \sqrt{p^G(x, y)q^G} \quad \text{and} \quad \rho^B = \sqrt{p^B(x, y)q^B}. \quad (3)$$

2.1.3. Keystone distortion

Major external distortion is brought by the rotation matrix defining the camcorder orientation. In other words, it arises when a three-dimensional object is projected on a plane. By this distortion, a square is transformed into a keystone (or trapezoid). It illustrated in Fig. 2.

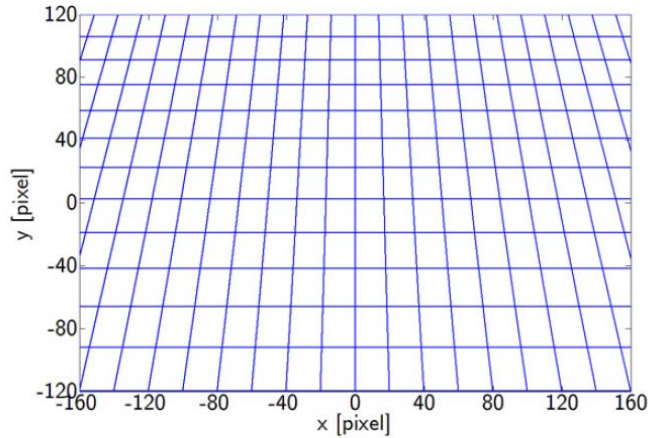


Fig. 2: Keystone distortion.

The keystone distortion is large enough to have serious effect on stability. Since an accurate measurement of the angle of the load swing is crucial for stabilization, the deviation of “zero” angle will cause a destructive effect. As mentioned earlier, this is a consequence of the way we mounted the handy camcorder. Although the camcorder orientation is adjustable and can be fixed by the screws, it is not suitable for fine tuning. It turned out that the desired precision in terms of the misalignment is beyond the tuning resolution of such a standard tripod.

A geometrical model for the projection distortion is shown in Fig. 3. A pinhole camera model is employed. Let F and f denote the focal point and the focal length, respectively. Ideally, the image plan S_I and S_M are perpendicular to the z -axis. The distance between S_I and S_M is denoted by d and let $f_d = f + d$.

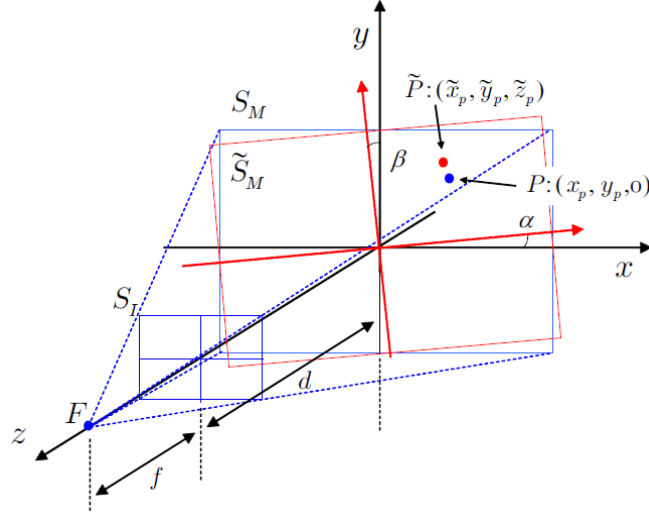


Fig. 3: Configuration for the projection distortion.

If the rotation happens, S_M rotated around y -axis by the amount of α and then rotated around x -axis by the amount of β as shown in the figure, then the new plane is made and denoted by \tilde{S}_M . So, if we have a point $P = (x_p, y_p, 0)$ on the plane S_M , then because of the rotation, the point will moves to $\tilde{P} = (\tilde{x}_p, \tilde{y}_p, \tilde{z}_p)$ on the \tilde{S}_M . Let $Q : (x_i, y_i)$ and $\tilde{Q} : (\tilde{x}_i, \tilde{y}_i)$ are the point in the images of P and \tilde{P} that observed from F . Then a simple geometrical calculation yields

$$\begin{bmatrix} x_i \\ y_i \end{bmatrix} = \frac{f}{f_d} \begin{bmatrix} x_p \\ y_p \end{bmatrix} \quad (4)$$

$$\text{and } \begin{bmatrix} \tilde{x}_i \\ \tilde{y}_i \end{bmatrix} = \frac{f}{\tilde{f}} \begin{bmatrix} x_p \cos \alpha - y_p \sin \alpha \sin \beta \\ y_p \cos \beta \end{bmatrix} \quad (5)$$

where $\tilde{f} = x_p \sin \alpha + y_p \cos \alpha \sin \beta + f_d$. By assuming that $\alpha \approx 0, \beta \approx 0$, then Eq. (5) can be rewritten as following

$$\begin{bmatrix} \tilde{x}_i \\ \tilde{y}_i \end{bmatrix} \approx \frac{f(x_p - y_p \alpha \beta)}{x_p \alpha + y_p \beta + f_d} \approx \left(1 - \frac{x_p \alpha + y_p \beta}{f_d} \right) \begin{bmatrix} x_i \\ y_i \end{bmatrix} \quad (6)$$

Suppose that l is the length of the wire in the upright position in S_M to be tracked, then the bottom end P_b and the top end P_t are located at $(x_c, 0, 0)$ and $(x_c, l, 0)$, respectively. Thus, after the axis rotation, the images of P_b and P_t are at

$$\begin{bmatrix} \frac{f}{f_d} x_c \left(1 - \frac{x_c \alpha}{f_d} \right) \\ 0 \end{bmatrix} \text{ and } \frac{f}{f_d} \left(1 - \frac{x_p \alpha + y_p \beta}{f_d} \right) \begin{bmatrix} x_c \\ l \end{bmatrix}, \quad (7)$$

respectively. The distortion angle offset is reasonably approximated by the following linear function of the load position:

$$\gamma = -\arctan \left(\frac{x_c \beta}{f_d - x_c \alpha - l \beta} \right) \approx -\frac{\beta}{f_d} x_c = \delta x_c \quad (8)$$

In Eq. (8), the distortion coefficient $\delta = -\beta / f_d$ [radian/m] quantifies the effect of the misalignment on the measurement error. In a practical case, we measure it in the image that captured by camcorder, then we need to convert δ from [radian/m] to [radian/pixel] by times with the resolution of the camcorder in [m/pixel].

2.2. Moving Visual Tracking

The configuration of the crane model is illustrated in Fig. 4. A two dimensional crane was built with a camcorder perpendicular to it. A visual tracking based on color histograms used to track the red wire and calculate the angle of the wire, also the position of the load. The object of the visual tracking is to measure θ and the positions of cart and the load.

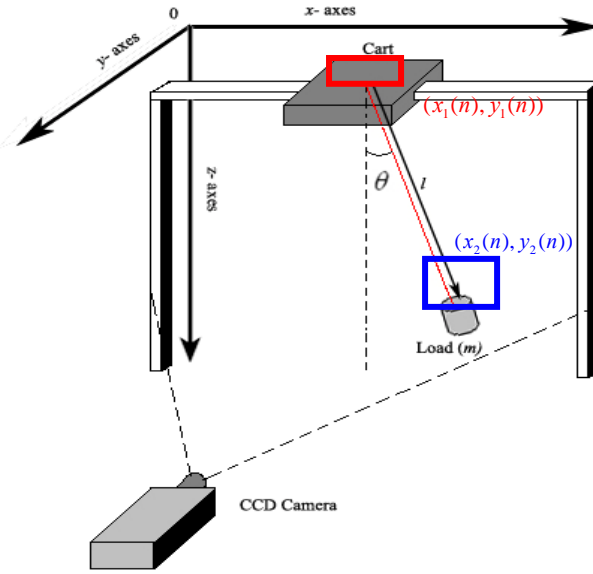


Fig. 4: Visual Tracking and Crane model.

Image processing task of tracking blocks instead of the whole image is proposed here to increase the computational speed. The tracking block is a rectangle, limited within length R_x pixels and width of R_y pixels covered the tracking point. The tracking point is the center of tracking patch, with the length and width H_x and H_y and must be smaller than the size of tracking block. Two tracking blocks are set to obtain the desired locations for calculation of the load swing. The distance between the first and the second tracking blocks determine the resolution of swing angle. So, we can put the first tracking point $(x_1(n), y_1(n))$ at the top of the rope (RED) and the second tracking point $(x_2(n), y_2(n))$ puts at the end of the rope to track the position of the load (BLUE), shown in Fig. 4. Tracking blocks also follow the tracking point movement. Since the processing area is small, the calculation time will be faster to achieve the maximum performance of the camcorder. When setting the speed of the tracking point movement in the image sequences, we know that fast movement needs a larger tracking area. However, the tracking area needs to be as small as it possible to produce shortest processing time, but one thing need to concern about is that the size of the tracking area is still able to catch the tracking

point. Besides, the center of the tracking patch has to follow the tracking point. The initial centers of two tracking patches are at the upper and lower ends of the wire and the centers of tracking patches move to the location of tracking points at next sampling time. Therefore, the centers of the tracking patches follow both the tracking points. Besides, the upper tracking block (RED) only moves along X -axis, so the size of R_y can be set to the smallest value equal to H_y . For the lower point $(x_2(n), y_2(n))$, the tracking point will follow the end of the wire. Because the load will be hoisted or lowered during the crane motion, the lower tracking point will move along both X - and Y - axis. Then, the size of the tracking block R_x and R_y must be larger than H_x and H_y .

Generating color histograms p^R, p^G, p^B within size (H_x, H_y) for each tracking position (x, y) inside the tracking blocks, we compare the color histograms of this model with the color histograms in the image sequences. The Bhattacharyya similarity measurement is used to measure the matching value of the color histograms. Then, these three similarities are blended to get a unified similarity as

$$\rho(x, y) = \eta\rho^R(x, y) + \mu\rho^G(x, y) + \nu\rho^B(x, y); \quad (9)$$

, where ρ^R, ρ^G and ρ^B are Bhattacharyya similarity coefficients and η, μ and ν are the positive weights of R, G and B colors satisfies $\eta + \mu + \nu = 1$. For an example, we set $\eta = 0.82, \mu = 0.09, \nu = 0.09$ and a solid color of red on the wire ($R = 255, G = 0, B = 0$). Suppose the red color is affected by shadow when moving, the new value of the color are $R = 240, G = 20, B = 20$. For the composition as shown in Eq. (9), it will not result in much different value of $\rho(x, y)$. But it still can be distinguished to the other color.

Then, comparing each value $\rho(x, y)$ in every position inside the tracking block will the ρ model, the point of $\rho(x, y)$ that has the closest value to the model will be the position of the target, that we called tracking point. Then, we can determine $(x_1(n), y_1(n))$ and $(x_2(n), y_2(n))$ which are the positions of the tracking

points in the image sequences.

After obtaining the position of the tracking points, we have the angle $\theta(n)$ of the wire with compensating the keystone distortion, defines as follows

$$\tan(\theta(n)) = \frac{\left((x_1(n) + \text{round}((y_1(n) - y_p)\tan(\delta x_1(n)))) - x_2(n) \right)}{(y_1(n) - y_2(n))} \quad (10)$$

Therefore, we can have the positions of tracking points and load swing angle by visual feedback with distortion compensation to be utilized in controller design.

2.3. Crane Controller Design

By Lagrange equations, we have the crane model as

$$(m_L + m_c)\ddot{x}_1 + m_L l(\ddot{x}_3 \cos x_3 - x_3^2 \sin x_3) + m_L \sin x_3 \ddot{l} + 2m_L \cos x_3 \dot{l}\dot{x}_3 + w_1(\mathbf{x}, t) = u \quad (11)$$

$$m_L l \ddot{x}_1 \cos x_3 + m_L l^2 \ddot{x}_3 + 2m_L l \dot{l} \dot{x}_3 + w_2(\mathbf{x}, t) = -m_L g l \sin x_3, \quad (12)$$

where m_c and m_L are the mass of crane system and the load, u is the control power to the crane motor. Let $\mathbf{x} = [x_1, x_2, x_3, x_4]^t = [r, \dot{r}, \theta, \dot{\theta}]^t$, g is gravity constant and $w_1(\mathbf{x}, t)$ and $w_2(\mathbf{x}, t)$ are external disturbance. So, we can have

$$\dot{\mathbf{x}} = A\mathbf{x} + B\mathbf{u} + D \quad (13)$$

by linearization, where

$$A = \begin{bmatrix} 0 & 1 & 0 & 0 \\ 0 & 0 & \frac{m_L}{m_c}g & 0 \\ 0 & 0 & 0 & 1 \\ 0 & 0 & -\frac{(m_L + m_c)g}{m_c l} & 0 \end{bmatrix}, \quad B = \begin{bmatrix} 0 \\ \frac{1}{m_c} \\ 0 \\ -\frac{1}{m_c l} \end{bmatrix}, \quad D = \begin{bmatrix} 0 \\ \frac{-w_1 l + w_2}{m_c l} \\ 0 \\ \frac{w_1 l - 2w_2}{m_c l^2} \end{bmatrix} = \begin{bmatrix} 0 \\ d_1 \\ 0 \\ d_2 \end{bmatrix}. \quad (14)$$

Therefore, we can use optimal based method [14],[15] to design the crane controller.

Let the performance index J is

$$J = \frac{1}{2} \mathbf{x}'(T)K(T)\mathbf{x}(T) + \frac{1}{2} \int_0^T (\mathbf{x}'Q(t)\mathbf{x} + uR(t)u)dt \quad (15)$$

during time period $[0, T]$, where $K(T)$ and $Q(t)$ are positive semi-definite weighting matrices, $R(t)$ is symmetric positive definite matrix and the Hamiltonian matrix is

$$H = \frac{1}{2} (\mathbf{x}'Q\mathbf{x} + u'Ru) + \lambda' (A\mathbf{x} + Bu) \quad (16)$$

$\lambda \in R^{4 \times 1}$ is the Lagrange constant with the states

$$\dot{\mathbf{x}} = H_{\lambda} = \frac{\partial H}{\partial \lambda} = A\mathbf{x} + Bu, \quad (17)$$

$$-\dot{\lambda} = H_x = \frac{\partial H}{\partial \mathbf{x}} = Q\mathbf{x} + A^T \lambda, \quad (18)$$

$$0 = H_u = \frac{\partial H}{\partial u} = Ru + B^T \lambda \quad (19)$$

So, we can derive the optimal control as

$$u(t) = -R^{-1} B^T \lambda \quad (20)$$

to verify the performance of controller by visual feedback. Besides, the power to hoisting and lowering the load has less effect on load swing, is controlled by general PID method.

參、實驗結果

Several experiments verify the effectiveness. The size of tracking blocks are 50 pixels for width and the length is 3 pixels for upper and 15 pixels for lower tracking blocks respectively. For the color tracking purpose, a red colored wire has been

placed on the crane model system. The resolution of image by our handy camcorder in these experiments is 720*480 pixels. Therefore the total computing load of using proposed tracking blocks are (3+15)*50 pixels, only about 1/400 of processing the whole image, suitable for real-time control application. The distance between the centers of upper and lower tracking blocks are 350 pixels, so the resolution of tracking load swing is

$$\theta = \tan^{-1}\left(\frac{1}{350}\right) = 0.16 \text{ deg.} \quad (21)$$

The following results verify the control performance by linear quadratic method with visual feedback. The mass of the crane system is about 30kg. The wire length is 1m. The external disturbance d_1 and d_2 are friction of track and nonlinear flexibility of wire. A handy camcorder, Sony PC-330, with 1394 card capture 30 frames per second. The image information are computed by Matlab in a personal computer with the CPU E4400 and DRAM 4G.

Figures 5-7 shows the experimental results. In Fig. 5, the weight of the load is 5kg. The solid line in Fig. 5(a) plots the cart motion along X-axis and the dashed line draws the hoisting and lowering of the load. The destination is set 0.7m. Figure 5(b) illustrates the load swing, Figures 5(c) and 5(d) represent the input power along horizontal and vertical axes. The maximum acceleration and velocity of the cart were set to 1.5625 m/s^2 and 0.225 m/s . It has shown that the maximum swing angle is 1.73 degrees. One can find the result by visual tracking is good.

Figure 6 shows the performance by using encoder as the position and anti-swing controller. The mass load is still 5kg and the destination is 0.7m too. The maximum acceleration and velocity of the cart were also set to 1.5625 m/s^2 and 0.225 m/s . It has shown that the maximum swing angle is 2.878 degrees. When compared with the results shown in Fig. 5, one can find the result by visual feedback is sensitive to small change; therefore, the overall payload swing is smaller. Though

the results by encoder look smooth; but the resolution is worse than visual feedback. It is the reason why the performance by visual feedback is better than those by encoder.

One also changes the weight of payload to 1kg to check the robustness of proposed visual feedback and linear quadratic control method. Destination, maximum acceleration and velocity of the cart were set the same with pervious cases. One can find the performance is still good. The maximum swing angle is 1.345 degrees.

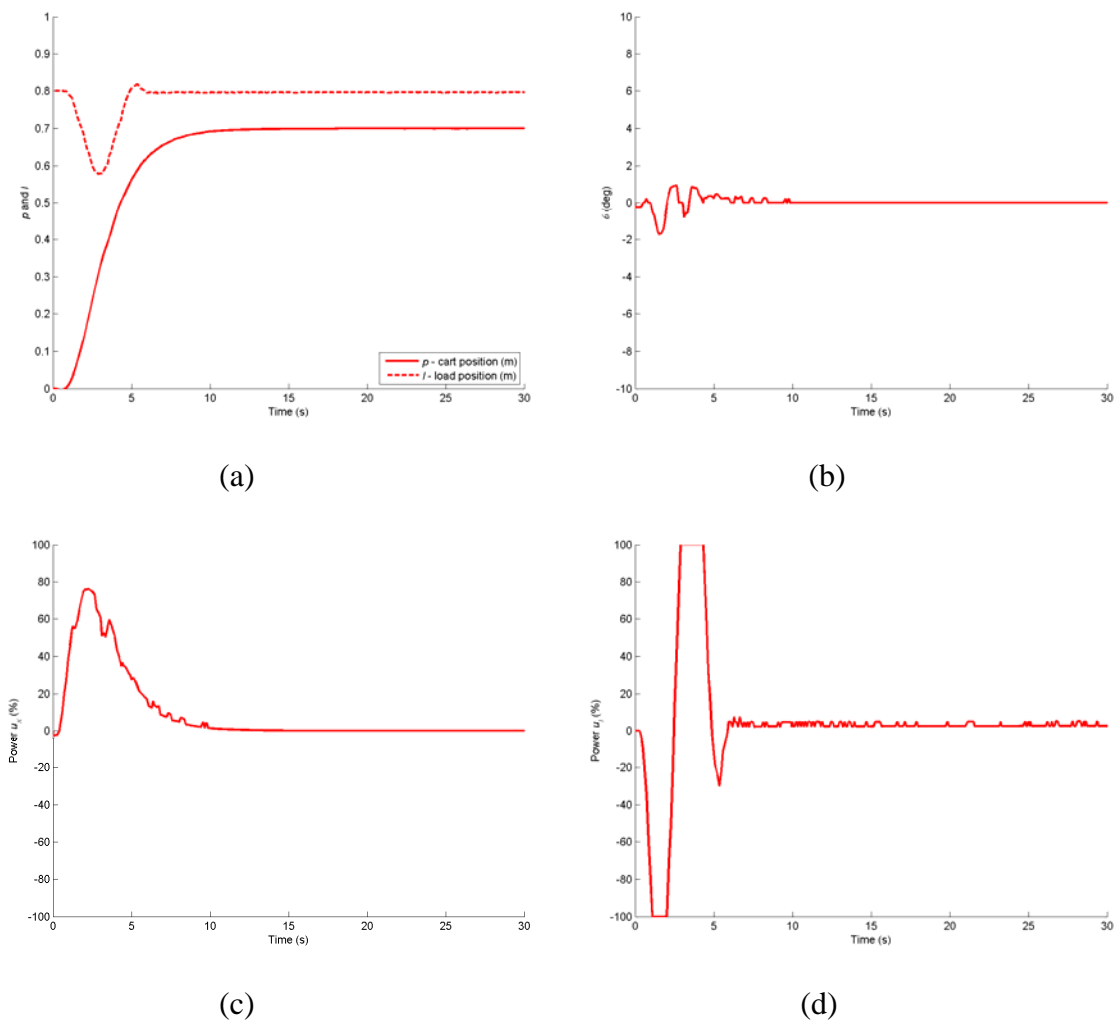
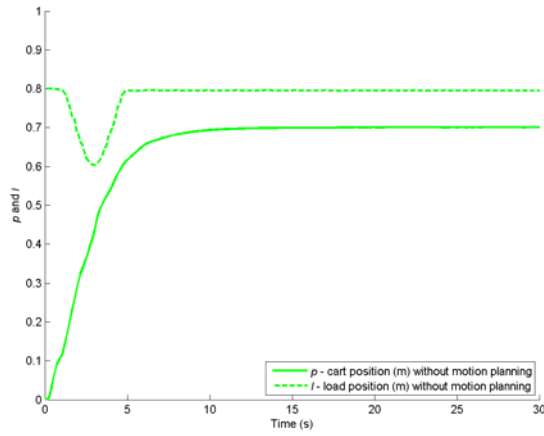
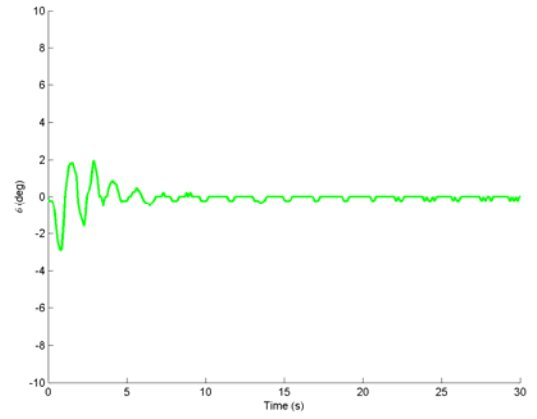


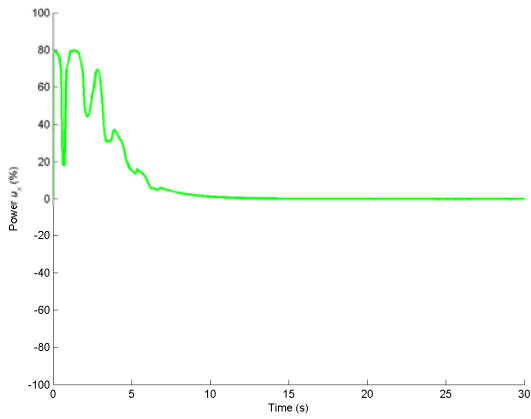
Fig. 5: Visual feedback control result, payload 5kg (a) cart position (b) load swing angle (c) horizontal input power (d) vertical input power.



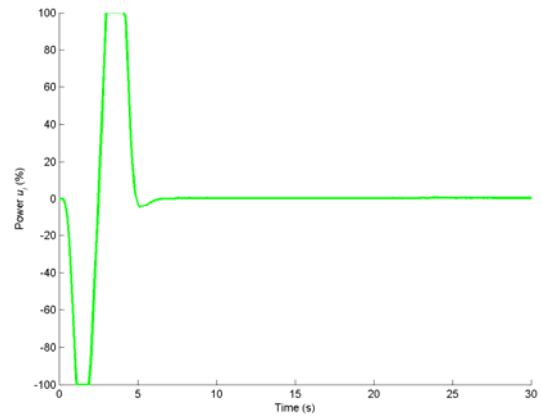
(a)



(b)

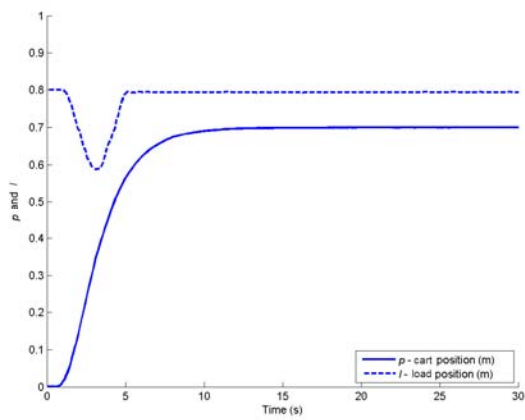


(c)

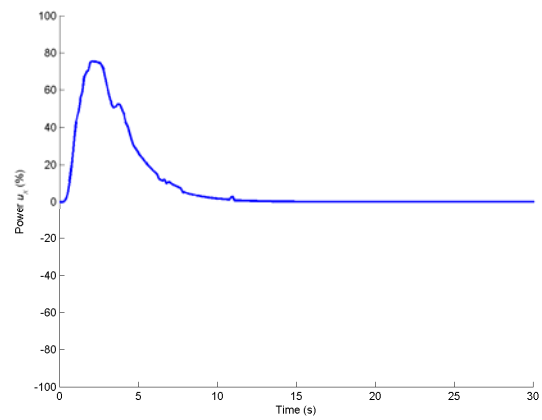


(d)

Fig. 6: Control result by encoder, payload 5kg (a) cart position (b) load swing angle (c) horizontal input power (d) vertical input power.



(a)



(c)

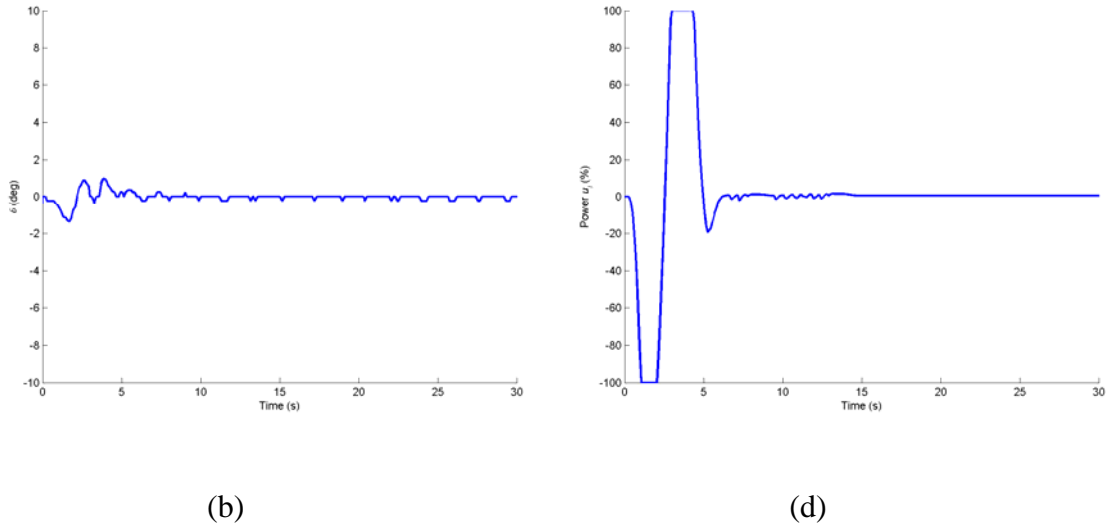


Fig. 7: Visual feedback control result, payload 1kg (a) cart position (b) load swing angle (c) horizontal input power (d) vertical input power.

肆、結論

A visual feedback method is proposed with a handy camcorder to replace conventional encoder in industrial applications. Image processing task with multi-tracking blocks only is also utilized to replace with processing the whole image frame. So, the proposed visual feedback methodology can control the crane in real-time. Experimental results show the performance by visual feedback is good under the disturbance. The image tracking method is discussed in this manuscript and is also versatile to the other industrial applications.

參考文獻

1. J. Ren, J. Orwell, G. A. Jones and M. Xu, "Tracking the soccer ball using multiple fixed cameras," *Computer Vision and Image Understanding*, vol. 113, no. 5, pp. 633-642, 2009.
2. F. Farivar, M. A. Shoorehdeli, M. Teshnehlab, "An interdisciplinary overview and intelligent control of human prosthetic eye movements system for the emotional support by a huggable pet-type robot from a biomechatrical viewpoint," *Journal of the Franklin Institute*, vol. 349, no. 7, pp. 2243-2267, 2012.
3. A. R. J. François, E. Chew, and D. Thurmond, "Performer-centered visual feedback for human-machine improvisation," *Computers in Entertainment*, vol. 9, no. 3, pp.13-13, 2011.
4. K. Kamejima, "Multi-fractal articulation of environmental saliency for contextual visualization," *International Journal of Innovative Computing, Information and Control*, vol. 8, no. 3(B), pp. 2233-2248, March 2012.
5. W. Yu, M. A. Moreno-Armendariz, "Robust visual servoing of robot manipulators with neuro compensation," *Journal of the Franklin Institute*, vol. 342, no. 7, pp. 824-838, 2005.
6. G. G. Rigatos, "A derivative-free distributed filtering approach for sensorless control of nonlinear systems," *International Journal of Systems Science*, vol. 43, no. 9, pp. 1699-1712, 2012.
7. H. P. Wang, C. Vasseur, A. Chamroo, V. Koncar, "Hybrid control for vision based cart-inverted pendulum system," *Proc. of the American Control Conf.*, pp. 3845-3850, 2008.
8. G. M. Chen, P. Z. Lin, W. Y. Wang, T. T. Lee, and C. H. Wang, "Image-based fuzzy control system," *Electronics Letters*, vol. 44, no. 7, pp. 461-462, 2008.
9. H. Kawai, Y. Choi, Y. B. Kim and Y. Kubota, "Measurement system design for sway motion based on image sensor", *Proc. of the 2009 IEEE International Conference on Networking, Sensing and Control*, pp. 185-188, 2009.

10. H. Osumi, A. Miura and S. Eiraku, "Positioning of wire suspension system using CCD cameras", *Proc. of IEEE/RSJ Int. Conf. Intell. Robots and Systems*, pp. 258-263, 2005.
11. D. Miyamoto, S. Nara and S. Takahashi, "Visual feedback control with laser for the position detection of crane hook", *SICE-ICASE International Joint Conf.*, pp. 2079- 2083, 2006.
12. T. Matsuo, R. Yoshino, H. Suemitsu and K. Nakano, "Nominal performance recovery by PID+Q controller and its application to antisway control of crane lifter with visual feedback," *IEEE Transactions on Control System Technology*, vol. 12, no. 1, pp. 156–166, 2004.
13. Y. Yoshida and K. Tsuzuki, "Visual tracking and control of a moving overhead crane load", *9th IEEE Int'l Conf. Advanced Motion Control*, pp. 630-635, 2006.
14. Y. C. Li and H. C. Liao, "The optimal parameter design for a blood supply chain system by the Taguchi method," *International Journal of Innovative Computing, Information and Control*, vol. 8, no. 11, pp. 7697-7712, 2012.
15. C. Jiang, K. L. Teo, R. Loxton and G. R. Duan, "A neighboring extremal solution for optimal switched impulsive control problems with large perturbations," *International Journal of Innovative Computing, Information and Control*, vol. 8, no. 9, pp. 6235-6258, 2012.

附錄：機械手臂之控制設計與模擬分析

機械手臂具有模仿人類手臂功能並可完成各種作業的自動控制設備。在工業自動化普及情況下已應用於各種工業上，可依照需求進而做到夾取、焊接、研磨等用途，如 Fig.A1。機械手臂為多輸入多輸出（MIMO）之非線性系統。因各功能的速度、精度、運動軌跡多有不同的需求，在選取適當的控制方法設計，是自動化產業不可或缺的技术。



Fig.A1. 機械手臂圖(摘自維基百科)

以兩軸式機械手臂為例，其示意圖如 Fig. A2，其中

m_1 ：第一軸機械臂質量

m_2 ：第二軸機械臂質量

I_1 ：第一軸機械臂質心處的慣性矩

I_2 ：第二軸機械臂質心處的慣性矩

l_1 ：第一軸機械臂的長度

l_2 ：第二軸機械臂的長度

l_{c1} ：第一軸軸心至質心的長度

l_{c2} ：第二軸軸心至質心的長度

θ_1 ：第一軸機械臂轉動的角度

θ_2 ：第二軸機械臂相對於第一軸臂轉動角度

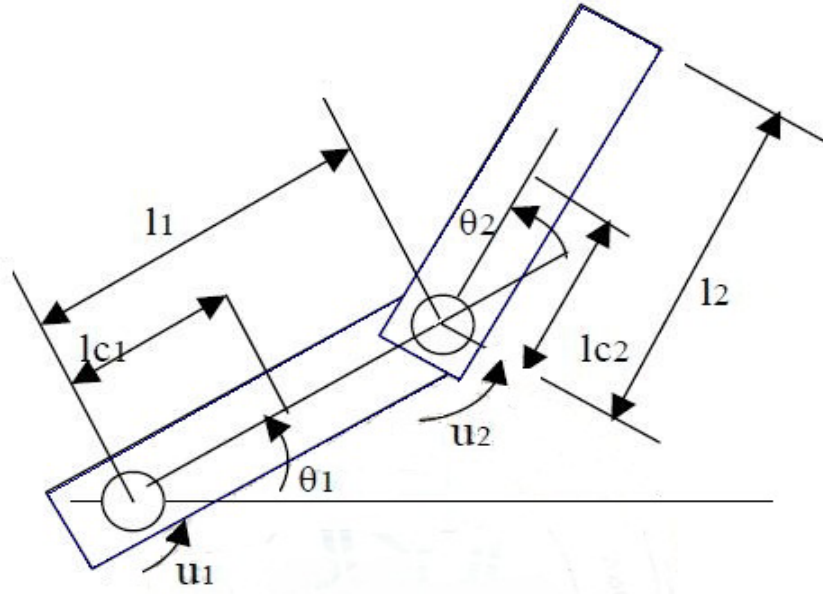


Fig. A2. 兩軸式機械手臂示意圖

此機械手臂動態方程式則可以下列 Lagrange 方程式來說明：

$$L = T - V$$

$$T = \frac{1}{2}I_1\dot{\theta}_1^2 + \frac{1}{2}m_1(l_{c1}\dot{\theta}_1)^2 + \frac{1}{2}I_2(\dot{\theta}_1 + \dot{\theta}_2)^2 + \frac{1}{2}m_2\{[l_1\dot{\theta}_1 + l_{c2}(\dot{\theta}_1 + \dot{\theta}_2)\cos\theta_2]^2 + [-l_{c2}(\dot{\theta}_1 + \dot{\theta}_2)\sin\theta_2]^2\}$$

$$V = m_1gl_{c1}\sin\theta_1 + m_2g[l_1\sin\theta_1 + l_{c2}\sin(\theta_1 + \theta_2)]$$

Lagrange's Equation :

$$\frac{d}{dt}\left(\frac{\partial L}{\partial \dot{\theta}_i}\right) - \frac{\partial L}{\partial \theta_i} = u_i \quad i=1,2$$

第一軸臂

$$\begin{aligned} \frac{d}{dt}\left(\frac{\partial L}{\partial \dot{\theta}_1}\right) &= \left[I_1 + I_2 + m_1l_{c1}^2 + m_2(l_1^2 + l_{c2}^2 + 2l_1l_{c2}\cos\theta_2) \right] \ddot{\theta}_1 \\ &+ (I_2 + m_2l_{c2}^2 + m_2l_1l_{c2}\cos\theta_2) \ddot{\theta}_2 - 2m_2l_1l_{c2}\dot{\theta}_1\dot{\theta}_2\sin\theta_2 - m_2l_1l_{c2}\dot{\theta}_2^2\sin\theta_2 \end{aligned}$$

$$\frac{\partial L}{\partial \theta_1} = -m_1gl_{c1}\cos\theta_1 - m_2gl_1\cos\theta_1 - m_2gl_{c2}\cos\theta_1\cos\theta_2 + m_2gl_{c2}\sin\theta_1\sin\theta_2$$

第二軸臂

$$\frac{d}{dt} \left(\frac{\partial L}{\partial \dot{\theta}_2} \right) = I_1 \ddot{\theta}_1 + I_2 \ddot{\theta}_2 + m_2 l_{c2}^2 \ddot{\theta}_2 + m_2 l_{c2}^2 \ddot{\theta}_1 + m_2 l_1 l_{c2} \ddot{\theta}_1 \cos \theta_2 - m_2 l_1 l_{c2} \dot{\theta}_1 \dot{\theta}_2 \sin \theta_2$$

$$\frac{\partial L}{\partial \theta_2} = -m_2 l_1 l_{c2} \dot{\theta}_1^2 \sin \theta_2 - m_2 l_1 l_{c2} \dot{\theta}_1 \dot{\theta}_2 \sin \theta_2 + m_2 g l_{c2} \sin \theta_1 \sin \theta_2 - m_2 g l_{c2} \cos \theta_1 \cos \theta_2$$

故經由上述推導，機械手臂的通式可以整合為下式：

$$H(\theta) \ddot{\theta} + C(\theta, \dot{\theta}) \dot{\theta} + g(\theta) = u$$

其中

$$H(\theta) = \begin{bmatrix} H_{11} & H_{12} \\ H_{21} & H_{22} \end{bmatrix}, C(\theta, \dot{\theta}) = \begin{bmatrix} -h\dot{\theta}_2 & -h\dot{\theta}_1 - h\dot{\theta}_2 \\ h\dot{\theta}_1 & 0 \end{bmatrix}, g(\theta) = \begin{bmatrix} g_1 \\ g_2 \end{bmatrix}, u = \begin{bmatrix} u_1 \\ u_2 \end{bmatrix}$$

$$H_{11} = I_1 + I_2 + m_1 l_{c1}^2 + m_2 (l_1^2 + l_{c2}^2 + 2l_1 l_{c2} \cos \theta_2)$$

$$H_{22} = I_2 + m_2 l_{c2}^2$$

$$H_{12} = H_{21} = I_2 + m_2 l_{c2}^2 + m_2 l_1 l_{c2} \cos \theta_2$$

且

$$h = m_2 l_1 l_{c2} \sin \theta_2$$

$$g_1 = m_1 l_{c1} g \cos \theta_1 + m_2 g [l_{c2} \cos(\theta_1 + \theta_2) + l_1 \cos \theta_1]$$

$$g_2 = m_2 l_{c2} g \cos(\theta_1 + \theta_2).$$

傳統的機械手臂控制設計可以參考 Fig. A3，在此，感測器量取機械手臂的旋轉角度值 θ_i 後回傳， θ_{di} 則是設定機械手臂要到達的角度，其中 $i \in \{1, 2\}$ ，如此，我們可以透過控制器的設定來使誤差值 e 達到最小。

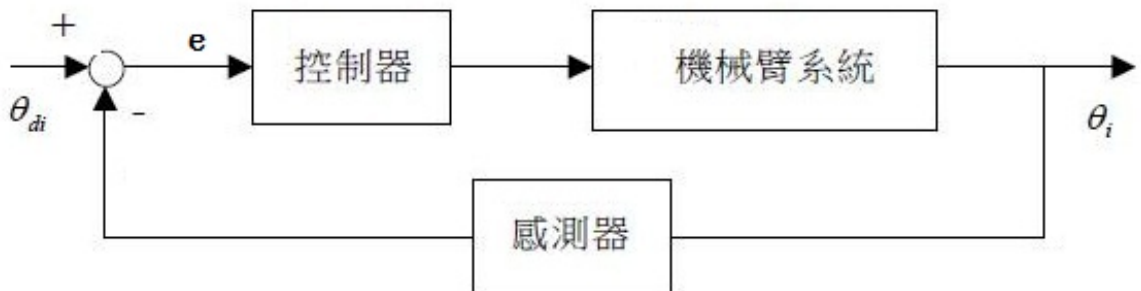


Fig. A3. 機械手臂控制示意圖

在本計畫中，控制器將使用比例-微分(PD)方式與滑動模式控制來設計，並比較其控制差異。所使用的機械手臂參數為

$$m_1=9.78 \text{ kg}, m_2=4.45 \text{ kg}, I_1=0.334 \text{ kg}\cdot\text{m}^2, I_2=0.063 \text{ kg}\cdot\text{m}^2$$

$l_1=0.359\text{ m}$, $l_2=0.240\text{ m}$, $l_{c1}=0.1360\text{ m}$, $l_{c2}=0.1020\text{ m}$
模擬結果如下所示：

Part1.比例-微分法：

比例微分法為工業上常用的控制方法，其優點為簡單、好用；惟所需參數常以嘗試錯誤法得到。在本計畫中以 PD 方式進行兩軸式機械手臂來做控制，其控制命令為

$$u(t) = k_p e(t) + k_d \dot{e}(t)$$

首先實驗以固定 $k_d = 15$ 的方式來探討 k_p 值對控制的影響，並分別在第 2、5 秒末對第一軸的設定角度，第 3、5 秒末對第二軸的設定角度分別做改變，以測試 PD 方法的追蹤效果，其結果如 Fig. A4 所示。其中， $(k_{p1}, k_{p2}, k_{p3}) = (35, 90, 15)$ ，由圖可見，若同時要求定位誤差與超越量(Overshoot)達到最小，在上述實驗將以 $k_p = 35$ 為宜。其對應的控制力則如 Fig. A5 所示。

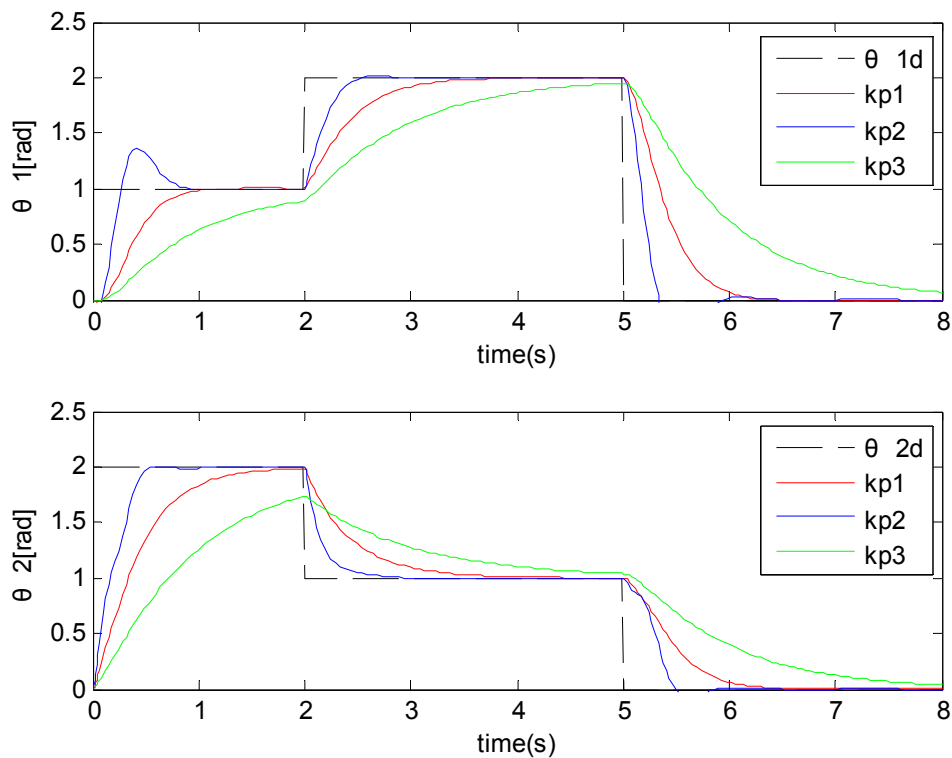


Fig. A4. 機械手臂控制結果，第一軸(上)，第二軸(下)

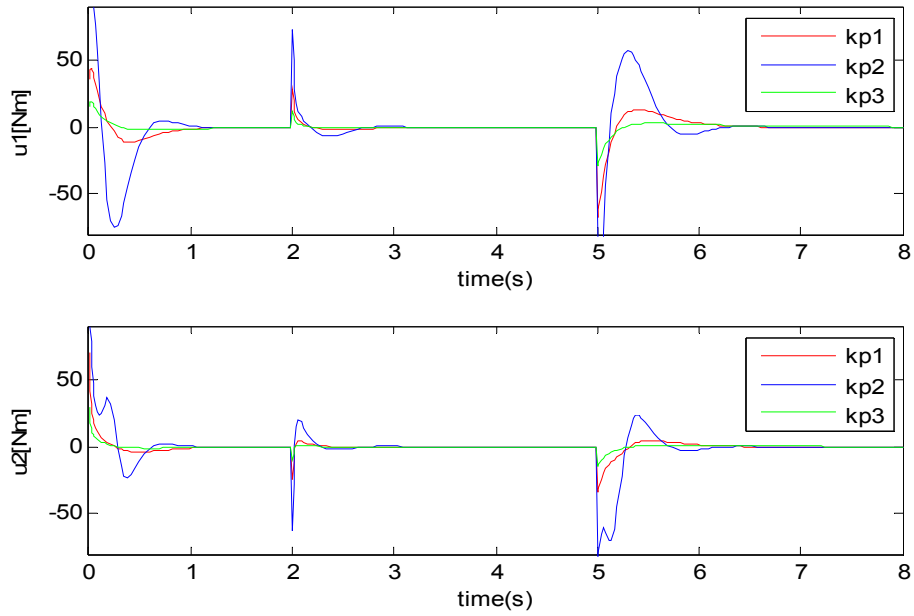


Fig. A5. 機械手臂控制力，第一軸(上)，第二軸(下)

由於前一結果發現 $k_p = 35$ 時有最佳的結果；因此，在接下來的實驗中將固定 $k_p = 35$ 來探討 $(k_{d1}, k_{d2}, k_{d3}) = (15, 25, 8)$ 對系統控制的影響，其結果如 Fig. A6 與 Fig. A7。

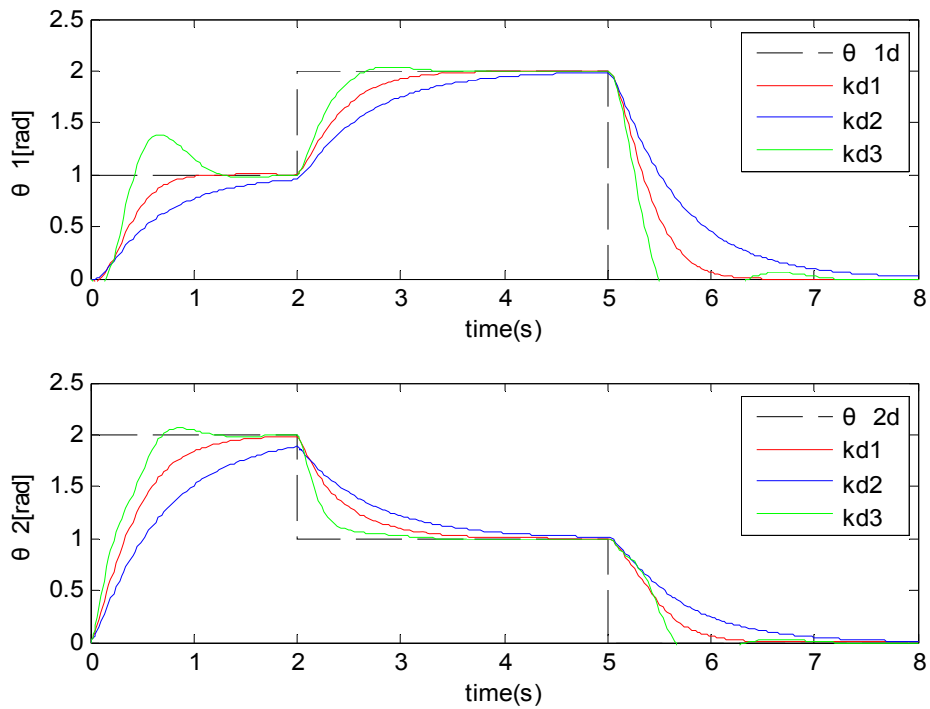


Fig. A6. 機械手臂控制結果，第一軸(上)，第二軸(下)

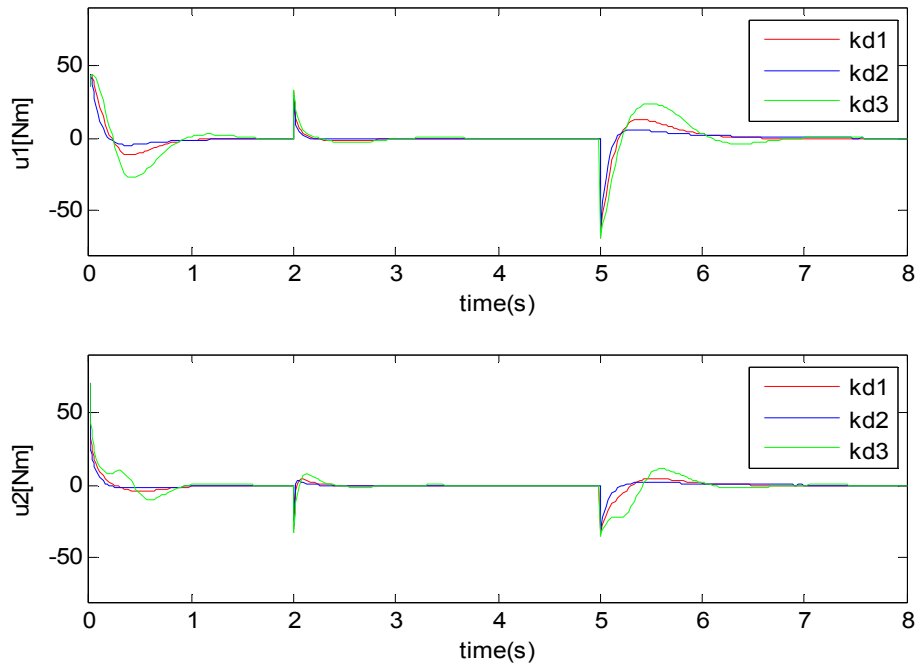


Fig. A7. 機械手臂控制力，第一軸(上)，第二軸(下)

由上述之實驗圖發現，控制增益參數的影響不僅是性能上的差異，亦可能造成不穩定的情況發生。故選擇一適當參數在各操作情況下完成誤差收斂是很重要的。總括來說，各參數的影響如下

k_p ：越大響應速度越快易影響穩定性。

k_d ：以誤差的斜率預測誤差方向，提高系統穩定性。

故 PD 控制設計可經由實驗測試，在穩定與速度間求其平衡，而在一些研究中也利用控制工程學概念分析系統響應變化，並做適當推論及修改以達所需控制性能。

Part 2. 滑動模式控制：

滑動模式控制(sliding mode control, SMC)，經過長年發展已成為相對獨立的研究分支，成為自動控制系統的一種設計方法。適用於線性與非線性系統、連續與離散系統、確定與不確定系統等。時常運用在運動控制中並廣泛在實際工程上得到應用。主要概念為迫使系統按照預定的狀態軌跡運動，其優點為系統在參數變動及外在干擾下，可透過控制量的切換使系統沿著滑動面滑動進而達到預期控制效果。

根據受控系統設計滑模面為 $s = ce(t) + \dot{e}(t)$ ，並透過 Lyapunov theorem 證明控制設計穩定性，欲達到理想滑模控制令 $\dot{s} = 0$ 。整體控制命令為 $u = u_{eq} + u_c$ 。

其中 u_{eq} 為等效控制可根據受控系統推算得知，主要作為滑模運動； u_c 為切換控制以 $sign$ 函數最為常見，其功能為強制切換至滑動面加強不確定性及干擾。 $sign$ 函數像是個理想的開關特性有著快速切換的效果，實際上系統卻會因為快速切換而造成控制力輸出的高頻率抖震，為了減少抖震現象在此控制器的設計採用的是 $sigmoid$ function。將設計完成的 SMC 與 PD 控制器做實驗比較，受控體為相同的兩軸式機械手臂，模擬實驗結果為 Fig. A8。為了驗證滑模控制的強健性，再以外加干擾實驗並與 PD 控制作比較，如圖 Fig. A9 所示。

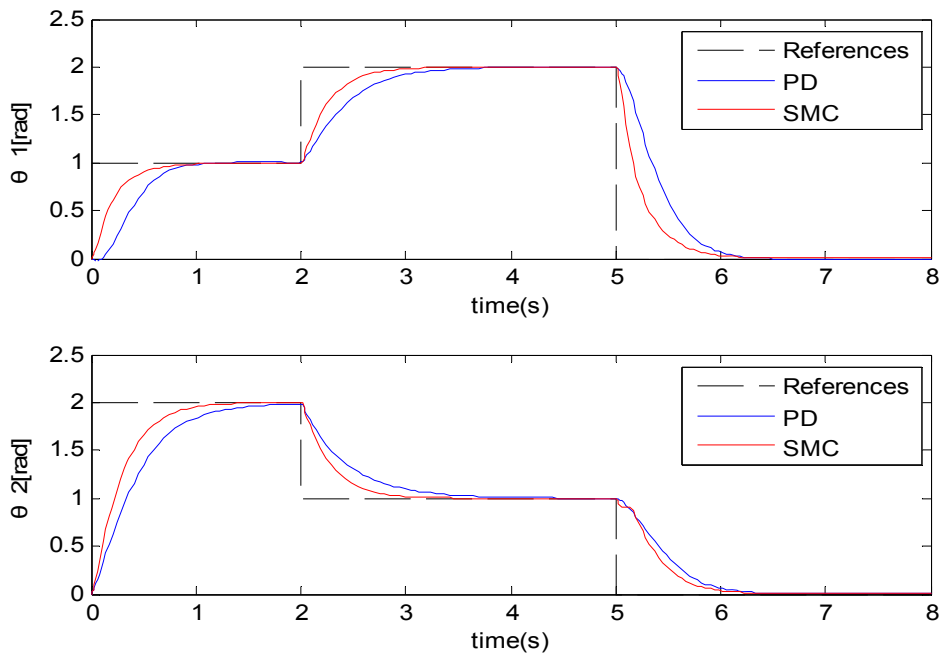


Fig. A8. 機械手臂控制結果，第一軸(上)，第二軸(下)

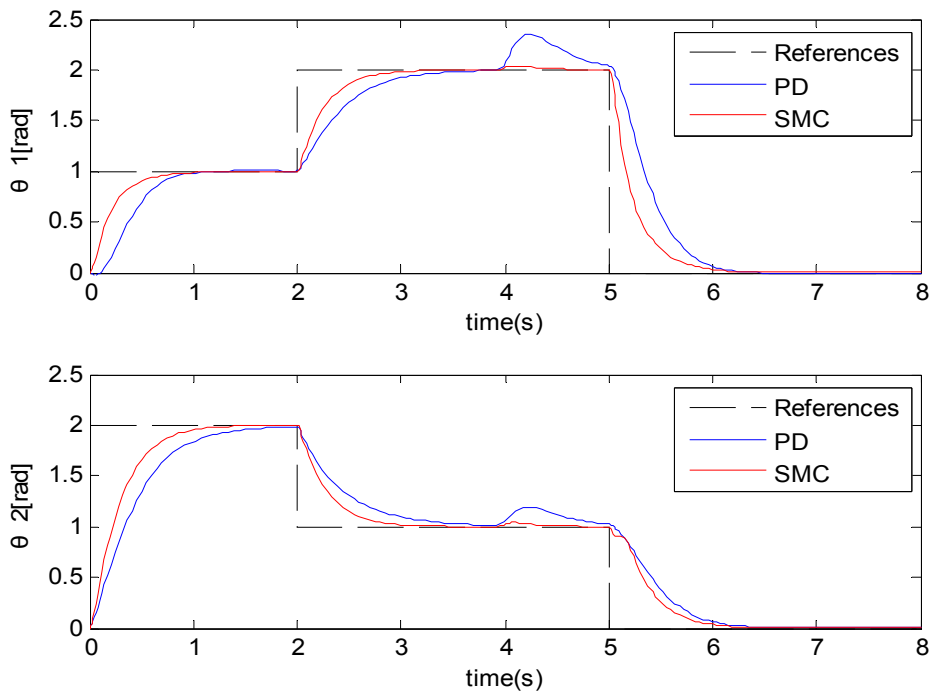


Fig. A9. 機械手臂控制外加干擾結果，第一軸(上)，第二軸(下)

上述之實驗結果顯示，以滑動模式控制其效果較為快速，並於在時間四秒時系統加入外部干擾，PD 控制受擾動影響幅度較大，反觀 SMC 在受到干擾時還能快速響應。接著我們再以弦波追蹤來驗證其效能。

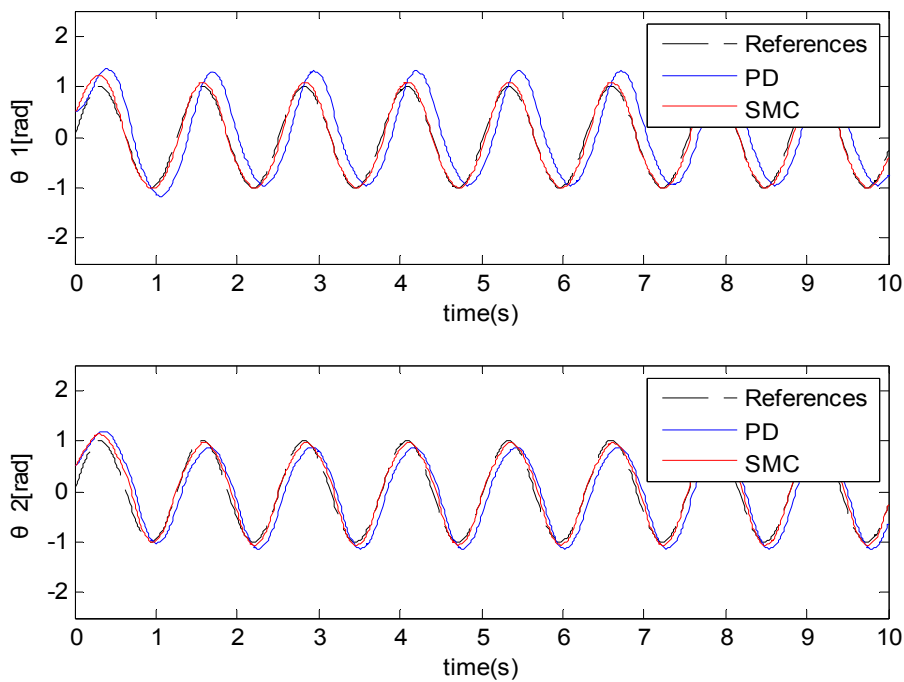


Fig. A10. 機械手臂控制週期性追蹤結果，第一軸(上)，第二軸(下)

由 Fig. A10 得知在同樣控制器情況下(初始值為 0.5)，面對弦波追蹤 SMC 的效果高出許多，而 PD 控制則需重新試驗取得新參數。然而各種控制器都有其優缺點，像 PD 成本較低易實現，控制性能需經驗調整特設計；SMC 則是控制輸出的有抖震現象，但是有著良好的強健性能。即使在外部干擾下響應速度快可立即做出反應，且在面對受控體參數的不確定下 SMC 控制性能較佳，意味著操作者不需重新設計參數即可準確快速地達到控制目標。